Electronic Supporting Information

Single-exponential solid-state delayed fluorescence decay in TADF compounds with minimized conformational disorder

Tomas Serevičius[a*], Rokas Skaisgiris[a], Irina Fiodorova[b], Gediminas Kreiza[a], Dovydas Banevičius[a], Karolis Kazlauskas[a], Sigitas Tumkevičius[b] and Saulius Juršėnas[a]

[a]Institute of Photonics and Nanotechnology, Vilnius University, Sauletekio 3, LT-10257 Vilnius, Lithuania.
[b]Institute of Chemistry Vilnius University, Naugarduko 24, LT-03225, Vilnius, Lithuania.
[*]Corresponding author: E-mail: tomas.serevicius@tmi.vu.lt

Table of Contents

Experimental section

Reagents and solvents were purchased directly from commercial suppliers; solvents were purified by known procedures. Melting points were determined in open capillaries with a digital melting point IA9100 series apparatus (ThermoFischer Scientific) and were not corrected. Thin layer chromatography was performed using TLC-aluminum sheets with silica gel (Merck 60 F254). Visualization was accomplished by UV light. Column chromatography was performed using Silica gel 60 (0.040-0.063 mm) (Merck). NMR spectra were recorded on a Bruker Ascend 400 (400 MHz and 100 MHz for ^{1}H and ^{13}C, respectively). ^{1}H NMR and ^{13}C NMR spectra were referenced to residual solvent peaks. Mass Spectrometry (HRMS) analyses were carried out on a quadrupole, time-of-flight mass spectrometer (microTOF-Q II, Bruker Daltonik GmbH, Bremen, Germany) or on Dual-ESI Q-TOF 6520 (Agilent Technologies) mass spectrometer. DSC curves were measured by Metler Toledo DSC1 apparatus, using aluminum crucibles under N_2 flow. Sample mass was around 8 – 10 mg, heating and cooling rates were 10 K/min. For X-Ray crystallography analysis, suitable crystals were selected and mounted on a glass fiber and analyzed on a XtaLab Synergy diffractometer equipped with HyPix-6000HE hybrid photon counting detector and PhotonJet microfocus X-ray source delivering CuKα (λ = 1.54184) radiation. X-ray measurements were carried out at room temperature. Data were collected and processed using CrysAlisPro software. Employing Olex2 graphical interface[1], the structures were solved by Intrinsic Phasing with the ShelXT[2] program and refined with the ShelXL[3] package using Least Squares minimization. The structure files of investigated crystals were deposited with the Cambridge Crystallographic Data Centre (**CCDC 2016464** (**Comp1**), **2014852** (**Comp2**), **2016478** (**Comp3**), **2010667** (**ACRPyr**)). These data can be obtained free of charge from the Cambridge Crystallographic Data Centre via www.ccdc.cam.ac.uk/data_request/cif. Photophysical properties were analysed in 1×10^{-5} M toluene solutions, 1 wt% PMMA, 3wt% DPEPO and TSPO1 films. 3 wt% doping concentration in DPEPO/TSPO1 was used to ensure the full energy transfer from host to emitter and simultaneously prevent the concentration quenching. Solid-state films were prepared by dissolving each material and host at appropriate ratios in toluene solutions and then wet-casting the solutions on quartz substrates. Absorption spectra were measured using Lambda 950 Uv/Vis spectrophotometer (PerkinElmer). Time-integrated fluorescence spectra (TIFL), time-resolved fluorescence spectra (TRFL), low-temperature phosphorescence (LTPH) spectra, fluorescence and phosphorescence decay transients were measured using nanosecond YAG:Nd^{3+} laser NT 242 (Ekspla, τ = 7 ns, pulse energy 200 μJ, repetition rate 1 kHz) and time-gated iCCD camera New iStar DH340T (Andor). Fluorescence transients were obtained by exponentially increasing delay and integration time[4]. Fluorescence quantum yields (Φ_{FL}, ±5% error) of the solutions and polymer films in air ambient were estimated using the integrated sphere method[5] by integrating sphere (Sphere Optics) connected to the CCD spectrometer PMA-12 (Hamamatsu) via optical fibre. Partially quenched TADF, existing in solid films in air-ambient, was excluded from Φ_{PF} values[6,7]. Solid-state samples were mounted in closed cycle He cryostat (Cryo Industries 204N) for all measurements (for oxygen-saturated and oxygen-free conditions). Toluene solutions were degassed by using freeze-pump-thaw method, 5 iterations. OLED device were fabricated on precleaned indium-tin oxide (ITO)-coated glass substrates. The small-molecule and cathode layers were thermally evaporated using vacuum evaporation apparatus (Vacuum Systems and Technologies Ltd) at $<6\times10^{-6}$ Torr pressure and deposition rate of about 1Å/s. OLED devices were encapsulated with a clear glass cover to prevent the interaction with ambient. Device current-voltage (*I-V*) characteristics and electroluminescence properties were measured using calibrated integrating sphere (Orb Optronics) and CCD spectrometer PMA-11 (Hamamatsu), powered by 2601A power supply unit (Keithley).

Quantum chemical calculations were performed by using density functional theory (DFT) as implemented in the Gaussian 09 software package at the B3LYP/6-31G(d) level[8]. Polarizable Continuum Model (PCM) was used to estimate the solvation behaviour of toluene surrounding.

Synthesis and characterization data of compounds

4,6-Bis(9,9-dimethyl-9,10-dihydroacridin-10-yl)pyrimidines (**ACRPyr**, **Comp1**, **Comp2** and **Comp3)** were synthesized using the corresponding 4,6-dichloropyrimidines **1**, **3** as starting materials by two step (**ACRPyr, Comp2**) or three step (**Comp1, Comp3**) protocols as depicted in scheme S1.

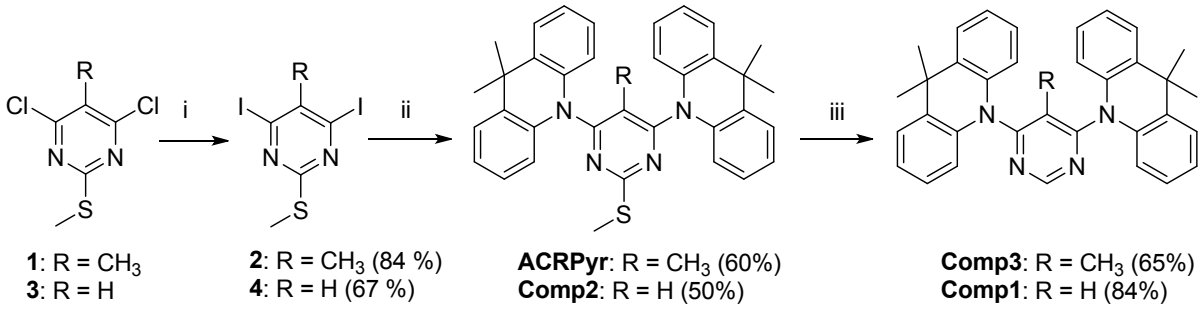

Scheme S1. Synthesis of **ACRPyr**, **Comp1**, **Comp2**, **and Comp3**. Reagents and conditions: i – 48 % HI, r.t., 72 h; ii – 9,9-dimethyl-9,10-dihydroacridine (2.2 equiv.), $Pd_2(dba)_3$ (7 mol%), $P(t\text{-}Bu)_3{\cdot}HBF_4$ (14 mol%), NaO*t*Bu (3.3 equiv.), toluene, 120 °C, 24 h, argon; iii – Raney Ni, methanol, reflux, 2 h.

4,6-Diiodo-5-methyl-2-methylthiopyrimidine (2). 4,6-Dichloro-5-methyl-2-methylthiopyrimidine (**1**) (240 mg, 1.15 mmol) in 48 % aqueous HI (5 mL) was stirred at 25 °C in the dark for 72 h. Water (50 mL) was added to the mixture and the aqueous solution was extracted with chloroform (4×25 mL). The combined extract was washed with 10 % aqueous Na_2CO_3 (2×25 mL), 5 % aqueous $Na_2S_2O_5$ (25 mL) and water (25 mL), then dried with anhydrous Na_2SO_4 and filtered. Chloroform was removed by distillation under reduced pressure. Residue was purified by filtration through SiO_2 layer using chloroform:petroleum ether (1:2) as an eluent to give compound **2**, which was used in the next step without further purification. Yield 380 mg (84 %) mp 123-125 °C. ^{1}H NMR ($CDCl_3$, 400 MHz) δ, ppm.: 2.53 (s, 3H, SCH_3), 2.61 (s, 3H, CH_3). ^{13}C NMR ($CDCl_3$, 100 MHz) δ, ppm: 14.45, 29.57, 132.18, 135.76, 169.97.

4,6-Diiodo-2-methylthiopyrimidine (4). Compound **4** was synthesized starting with 600 mg (3.08 mmol) of 4,6-dichloro-2-methylthiopyrimidine (**3**) according to the procedure described for the synthesis of compound **2**. Yield 787 mg (67 %), mp 153-155 °C. ^{1}H NMR ($CDCl_3$, 400 MHz) δ, ppm.: 2.45 (s, 3H, SCH_3), 7.78 (s, 1H, CH). ^{1}H NMR spectrum and mp of compound **4** match with those described in ref.[9].

5-Methyl-4,6-bis(9,9-dimethyl-9,10-dihydroacridin-10-yl)-2-methylthiopyrimidine (ACRPyr). 4,6-Diiodo-5-methyl-2-methylthiopyrimidine (**2**) (162.0 mg, 0.41 mmol), 9,9-dimethyl-9,10-dihydroacridine (190 mg, 0.91 mmol), $Pd_2(dba)_3$ (26.5 mg, 0.03 mmol, 7 mol%), $P(t\text{-}Bu)_3{\cdot}HBF_4$ (16.8 mg, 0.06 mmol, 14 mol%), NaO*t*Bu (130.9 mg, 1.36 mmol) and toluene (3 mL) were placed in a screw-cap vial equipped with a magnetic stir bar and purged with argon for 10 min. The reaction mixture was stirred at 120 °C for 24 h under argon atmosphere. After completion of the reaction, toluene was removed by distillation under reduced pressure, water (40 mL) was added to residue, and the aqueous solution was extracted with chloroform (4×25 mL). The combined

extract was dried with anhydrous Na_2SO_4 and filtered. Chloroform was removed by distillation under reduced pressure. Residue was purified by column chromatography using chloroform:petroleum ether (1:2) as an eluent and recrystallized from 2-propanol to give **ACRPyr**. Yield 138 mg (60 %), mp 167 °C (DSC data). ^{1}H NMR ($CDCl_3$, 400 MHz) δ, ppm.: 1.72 (s, 12H, CH_3-Acr), 1.82 (s, 3H, CH_3), 2.65 (s, 3H, SCH_3), 6.60 (dd, *J* = 8 Hz, *J* = 1 Hz, 4H, Acr-H), 7.06 (dt, *J* = 8 Hz, *J* = 1 Hz, 4H, Acr-H), 7.13 (dt, *J* = 8 Hz, *J* = 1 Hz, 4H, Acr-H), 7.53 (dd, *J* = 8 Hz, *J* = 1 Hz, 4H, Acr-H). ^{13}C NMR ($CDCl_3$, 100 MHz) δ, ppm: 11.9, 14.5, 31.5, 36.2, 113.8, 122.1, 124.9, 125.9, 126.8, 131.0, 138.1, 164.4, 173.0. HRMS-ESI: m/z calcd. for MH^+ ($C_{36}H_{35}N_4S$): 555.2577; found: 555.2571.

4,6-Bis(9,9-dimethyl-9,10-dihydroacridin-10-yl)pyrimidine (Comp1). 4,6-Bis-(9,9-dimethyl-9,10-dihydroacridin-10-yl)-2-methylthiopyrimidine (**Comp2**) (55 mg, 0.102 mmol), Raney Ni (165 mg, 2.8 mmol), prepared before reaction, and methanol (3 mL) were placed in a screw-cap vial equipped with a magnetic stir bar. The reaction mixture was heated at 80-85°C for 2 h. After completion of the reaction, Raney nickel was removed by filtration and washed with hot chloroform. The filtrate was concentrated to dryness under reduced pressure and the obtained residue was purified by column chromatography using chloroform as an eluent to give 42 mg (84 %) of **Comp1**, mp 270-271 °C. ^{1}H NMR ($CDCl_3$, 400 MHz) δ, ppm.: 1.51 (s, 12H, CH_3), 6.82 (s, 1H, Pyr-H), 7.20 (dt, *J* = 8 Hz, *J* = 1 Hz, 4H, Acr-H), 7.28 (dt, *J* = 8 Hz, *J* = 1 Hz, 4H, Acr-H), 7.45 (dd, *J* = 8 Hz, *J* = 1 Hz, 4H, Acr-H), 7.73 (dd, *J* = 8 Hz, *J* = 1 Hz, 4H, Acr-H), 8.56 (s, 1H, Pyr-H). ^{13}C NMR ($CDCl_3$, 100 MHz) δ, ppm.: 26.9, 37.8, 87.4, 123.7, 125.3, 125.4, 125.7, 139.4, 142.3, 158.3, 161.4. HRMS-ESI: m/z calcd. for MH^+ ($C_{34}H_{31}N_4$): 495.2549; found: 495.2542.

4,6-Bis(9,9-dimethyl-9,10-dihydroacridin-10-yl)-2-methylthiopyrimidine (Comp2). Comp2 was synthesized starting with 60.0 mg (0.16 mmol) of 4,6-diiodo-2-methylthiopyrimidine (**4**) according to the procedure described for the synthesis of compound **ACRPyr**. Yield 43 mg (50 %), mp 228-231 °C (from 2-propanol). ^{1}H NMR ($CDCl_3$, 400 MHz) δ, ppm.: 1.47 (s, 12H, CH_3), 2.52 (s, 3H, SCH_3), 6.35 (s, 1H, Pyr-H), 7.17 (dt, *J* = 8 Hz, *J* = 1 Hz, 4H, Acr-H), 7.24 (dt, *J* = 8 Hz, *J* = 1 Hz, 4H, Acr-H), 7.41 (dd, *J* = 8 Hz, *J* = 1 Hz, 4H, Acr-H), 7.76 (dd, *J* = 8 Hz, *J* = 1 Hz, 4H, Acr-H). ^{13}C NMR ($CDCl_3$, 100 MHz) δ, ppm: 14.4, 27.0, 37.7, 84.7, 123.4, 125.1, 125.48, 125.5, 139.4, 142.0, 161.2, 171.4. HRMS-ESI: m/z calcd. for MH^+ ($C_{35}H_{33}N_4S$): 541.2426; found: 541.2418.

5-Methyl-4,6-bis(9,9-dimethyl-9,10-dihydroacridin-10-yl)pyrimidine (Comp3). Comp3 was synthesized starting with 60.0 mg (0.16 mmol) of **ACRPyr** according to the procedure described for the synthesis of **Comp1**. Yield 36 mg (65 %), mp 214-217 °C. ^{1}H NMR ($CDCl_3$, 400 MHz) δ, ppm.: 1.72 (s, 12H, CH_3), 1.92 (s, 3H, CH_3), 6.46 (dd, *J* = 8 Hz, *J* = 1 Hz, 4H, Acr-H), 7.05 (dt, *J* = 7 Hz, *J* = 1 Hz, 4H, Acr-H), 7.11 (dt, *J* = 7 Hz, *J* = 2 Hz, 4H, Acr-H), 7.53 (dd, *J* = 8 Hz, *J* = 2 Hz, 4H, Acr-H), 9.51 (s, 1H, Pyr-H). ^{13}C NMR ($CDCl_3$, 100 MHz) δ, ppm.: 12.34, 31.54, 36.15, 113.55, 122.13, 126.01, 126.80, 131.02, 131.72, 138.10, 159.66, 164.59. HRMS-ESI: m/z calcd. for MH^+ ($C_{35}H_{33}N_4$): 509.2705; found: 509.2698.

5-Methyl-4,6-bis[4-(9,9-dimethyl-9,10-dihydroacridin-10-yl)phenyl]-2-methylthiopyrimidine (ACRphenPyr) was synthesized by the Suzuki cross-coupling reaction of 4,6-diiodopyrimidine 2 with 4-bromophenylboronic acid and following Buchwald-Hartwig amination reaction of the obtained intermediate **5** with 10,10-dimethyl-9,10-dihydroacridine (Scheme S2).

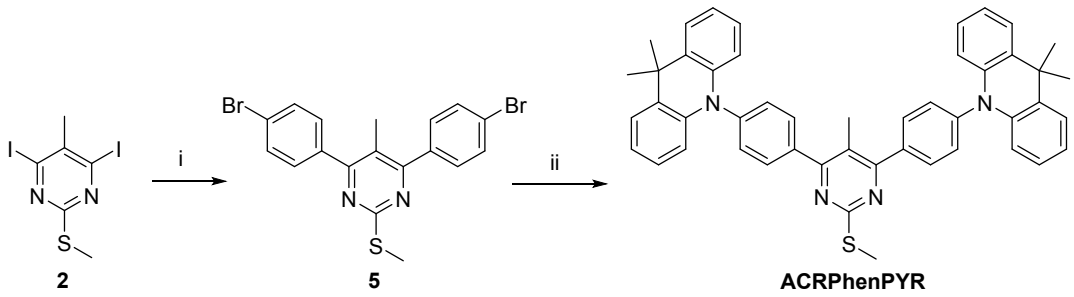

2 **5** **ACRPhenPYR**

Scheme S2. Synthesis of 5-methyl-4,6-bis[4-(9,9-dimethyl-9,10-dihydroacridin-10-yl)phenyl]-2-methylthiopyrimidine **(ACRphenPyr)**. Reagents and conditions: i – 4-bromophenylboronic acid (2.4 equiv.), $Pd(PPh_3)_2Cl_2$ (5 mol%), K_3PO_4 (7.2 equiv.), toluene, 150 °C, 18 h; ii – 9,9-dimethyl-9,10-dihydroacridine (2.2 equiv.), $Pd_2(dba)_3$ (5 mol%), P(*t*Bu)$_3$·HBF_4 (10 mol%), NaO*t*Bu (3.3 equiv.), toluene, 150 °C, 24 h, argon.

5-Methyl-4,6-bis(4-bromophenyl)-2-methylthiopyrimidine (**5**). 4,6-Diiodo-5-methyl-2-methylthiopyrimidine (**2**) (120 mg, 0.31 mmol), 4-bromophenylboronic acid (147.6 mg, 0.73 mmol), $Pd(PPh_3)_2Cl_2$ (17.6 mg, 5 mol%), K_3PO_4 (467.4 mg, 2.20 mmol) and toluene (4 mL) were placed in a screw-cap vial equipped with a magnetic stir bar and purged with argon for 10 min. The reaction mixture was stirred at 150 °C for 18 h under argon atmosphere. After completion of the reaction, toluene was removed by distillation under reduced pressure. Water (40 mL) was added to the residue and the aqueous solution was extracted with chloroform (4×25 mL). The extract was dried with anhydrous Na_2SO_4, filtered, and chloroform was removed by distillation under reduced pressure. Residue was purified by column chromatography using chloroform:petroleum ether (1:1) as an eluent to give 94 mg (68%) of compound **5**, mp 148-150 °C (from 2-propanol). ^{1}H NMR ($CDCl_3$, 400 MHz) δ, ppm.: 2.30 (s, 3H, Me), 2.63 (s, 3H, SMe), 7.56 (d, J = 8 Hz, 4H, CH), 7.66 (d, J = 8 Hz, 4H, CH). ^{13}C NMR ($CDCl_3$, 100 MHz) δ, ppm.: 14.3, 17.2, 120.1, 123.9, 130.8, 131.6, 137.3, 166.1, 169.2. HRMS-ESI: m/z calcd. for MH^+ ($C_{18}H_{15}Br_2N_2S$): 450.9302; found: 450.9297.

5-Methyl-4,6-bis[4-(9,9-di-methyl-9,10-dihydroacridin-10-yl)phenyl]-2-methylthiopyrimidine (ACRphenPyr). 4,6-Bis(4-bromophenyl)-2-methylthio-5-methylpyrimidine (**5**) (43.7 mg, 0.1 mmol), 9,9-di-methyl-9,10-dihydroacridine (44.7 mg, 0.21 mmol), Pd_2dba_3 (4.5 mg, 5 mol%), P(*t*Bu)$_3$·HBF_4 (2.8 mg, 10 mol%), NaO*t*Bu (30.8 mg, 0.3205 mmol) and toluene (2 mL) were placed in a screw-cap vial, equipped with a magnetic stir bar. The reaction mixture was purged with argon for 10 min and stirred at 150 °C for 24 h under argon atmosphere. After completion of the reaction, toluene was removed by distillation under reduced pressure. Residue was purified by column chromatography using chloroform:petroleum ether (1:1) as an eluent to give 41,2 mg (60 %) of **ACRphenPyr**, mp 239-241°C (from 2-propanol). ^{1}H NMR ($CDCl_3$, 400 MHz) δ, ppm.: 1.74 (s, 12H, CH_3), 2.55 (s, 3H, SCH_3), 2.76 (s, 3H, CH_3), 6.41 (d, J = 8 Hz, 4H, Acr-H), 6.97-7.07 (m, 8H, Acr-H), 7.49-7.56 (m, 8H, CH), 8.00 (d, J = 8 Hz, 4H, Acr-H). ^{13}C NMR ($CDCl_3$, 100 MHz) δ, ppm.: 14.5, 17.8, 31.2, 36.1, 114.2, 120.5, 120.9, 125.3, 126.4, 130.3, 131.3, 132.0, 138.0, 140.7, 142.6, 166.5, 169.2. HRMS-ESI: m/z calcd. for MH^+ ($C_{48}H_{43}N_4S$): 707.3209; found: 707.3202.

^{1}H and ^{13}C NMR spectra of the synthesized compounds.

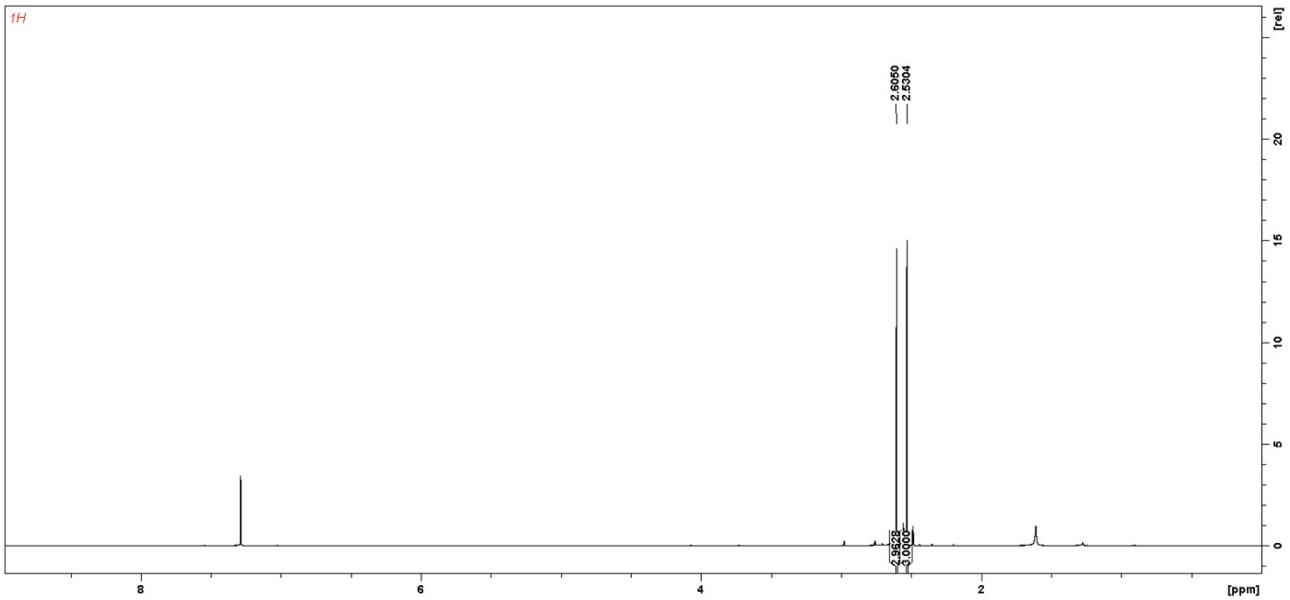

Fig. S1. ^{1}H NMR spectrum of 4,6-diiodo-5-methyl-2-methylthiopyrimidine (**2**) in $CDCl_3$.

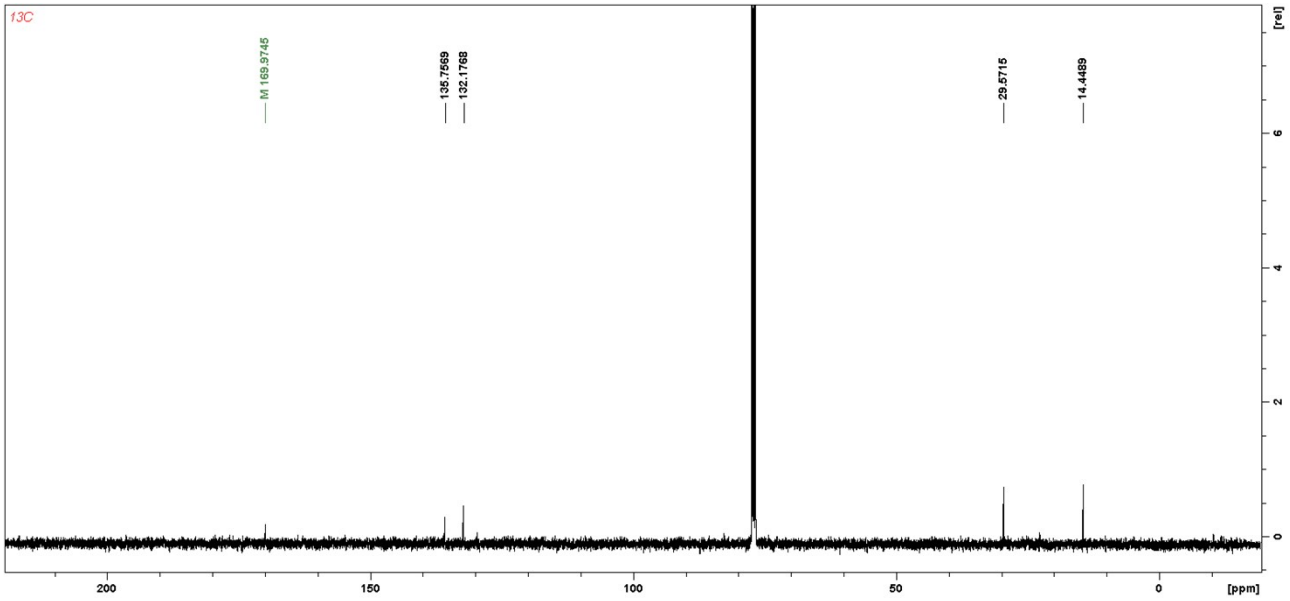

Fig. S2. ^{13}C NMR spectrum of 4,6-diiodo-5-methyl-2-methylthiopyrimidine (**2**) in $CDCl_3$.

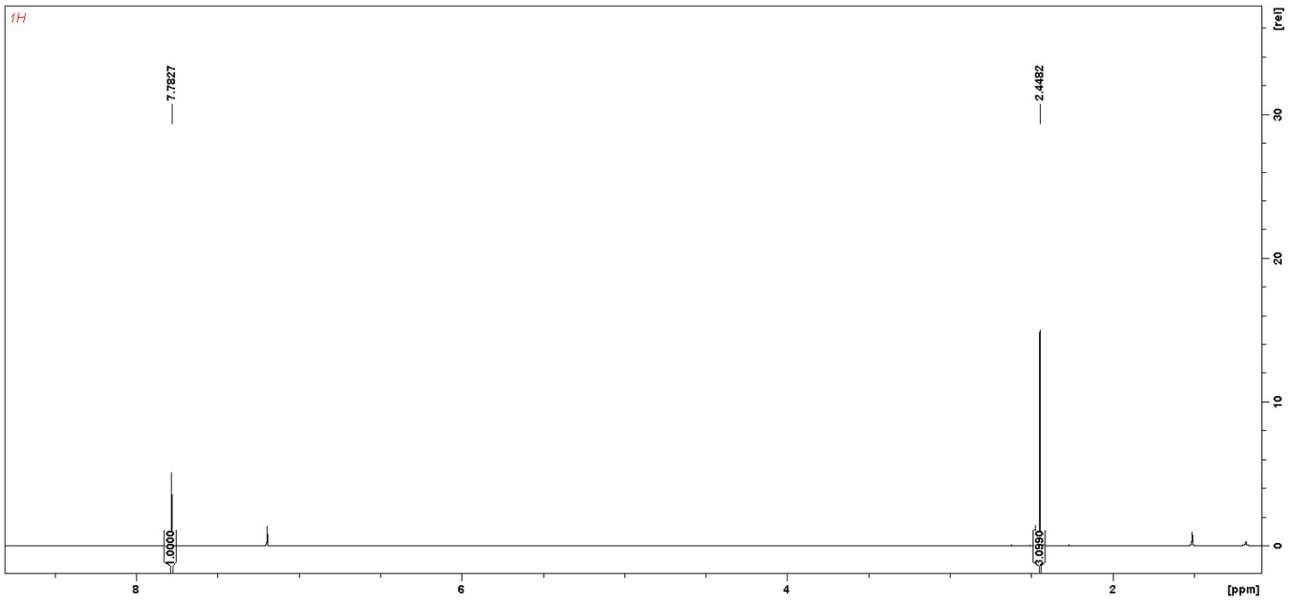

Fig. S3. ^{1}H NMR spectrum of 4,6-diiodo-2-methylthiopyrimidine (**4**) in $CDCl_3$.

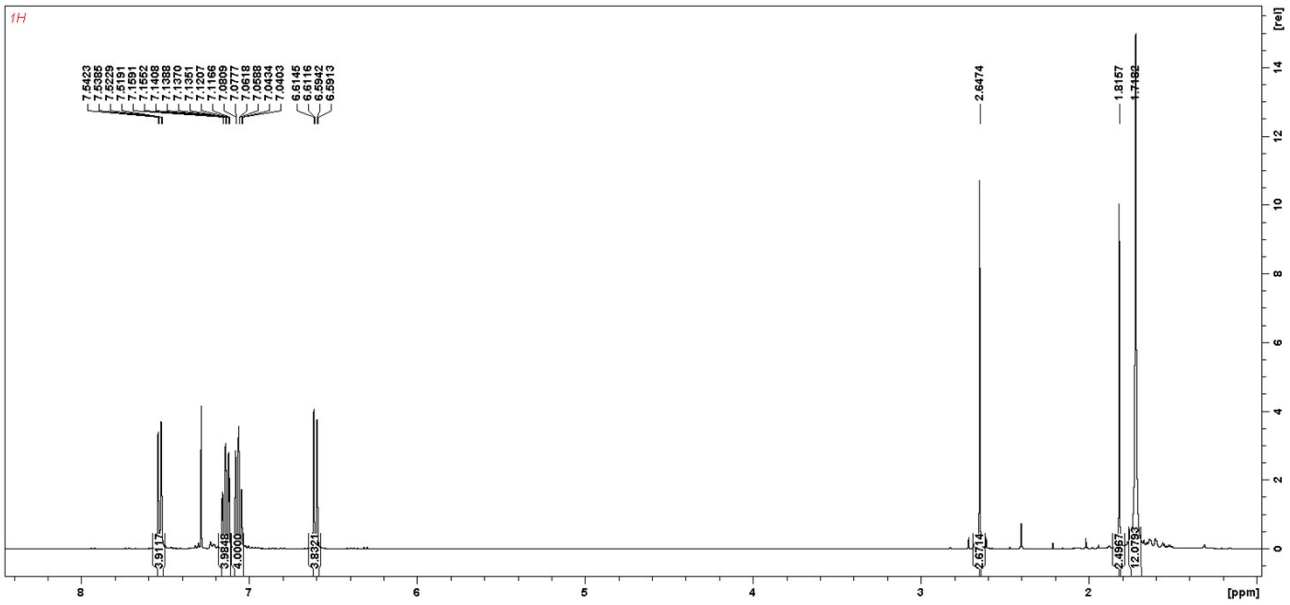

Fig. S4. ^{1}H NMR spectrum of 5-methyl-4,6-bis(9,9-dimethyl-9,10-dihydroacridin-10-yl)-2-methylthiopyrimidine (**ACRPyr**).

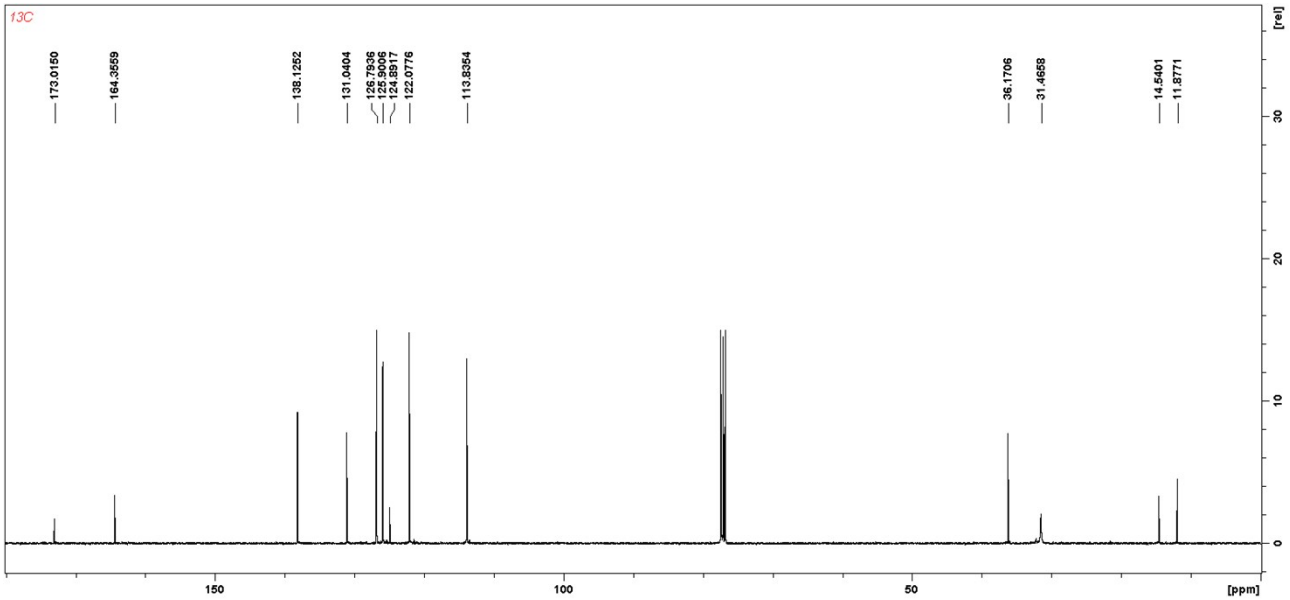

Fig. S5. ^{13}C NMR spectrum of 5-methyl-4,6-bis(9,9-dimethyl-9,10-dihydroacridin-10-yl)-2-methylthiopyrimidine (**ACRPyr**).

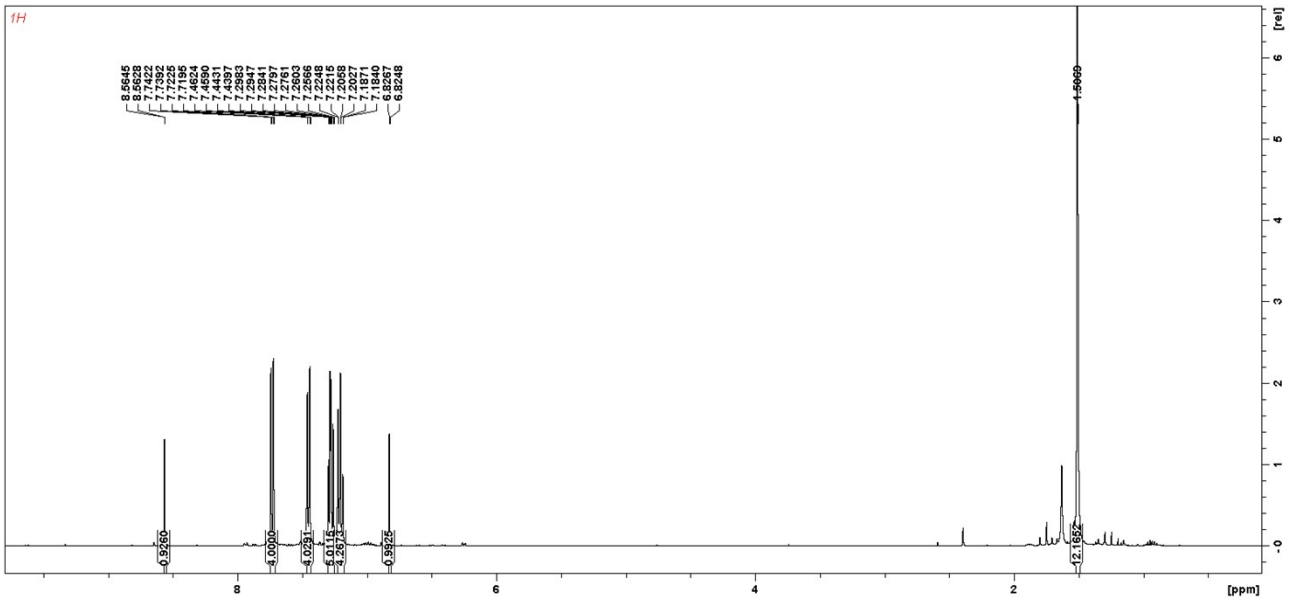

Fig. S6. ^{1}H NMR spectrum of 4,6-bis(9,9-dimethyl-9,10-dihydroacridin-10-yl)pyrimidine (**Comp1**).

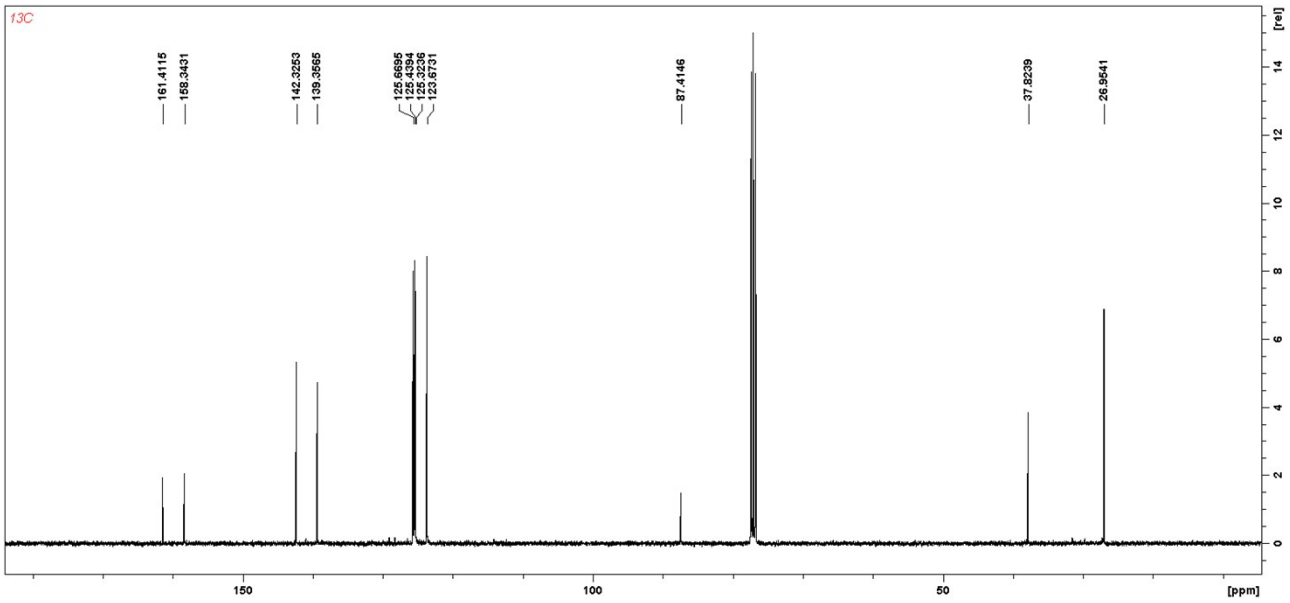

Fig. S7. ^{13}C NMR spectrum of 4,6-bis(9,9-dimethyl-9,10-dihydroacridin-10-yl)pyrimidine (**Comp1**).

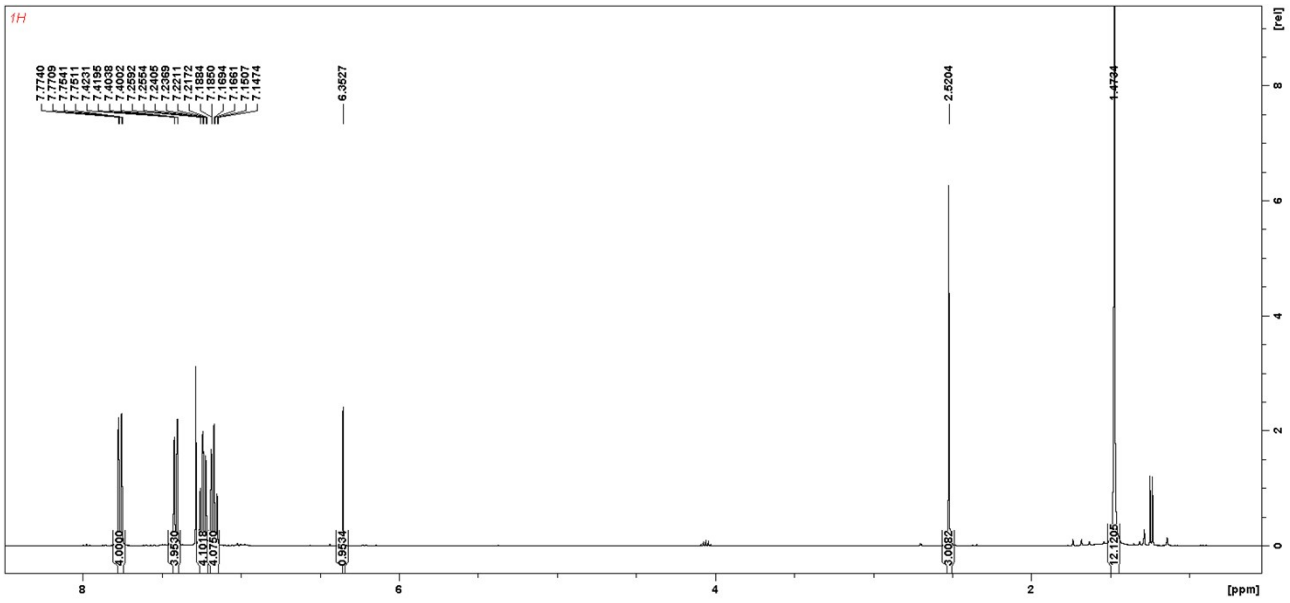

Fig. S8. ^{1}H NMR spectrum of 4,6-bis(9,9-dimethyl-9,10-dihydroacridin-10-yl)-2-methylthiopyrimidine (**Comp2**).

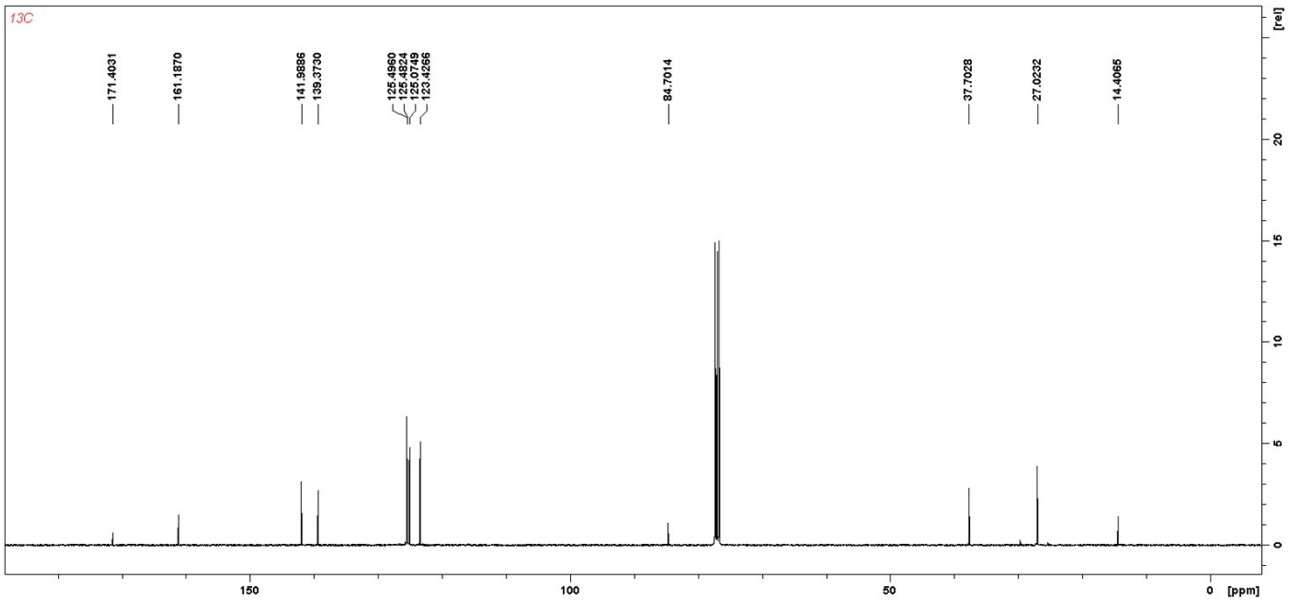

Fig. S9. ^{13}C NMR spectrum of 4,6-bis(9,9-dimethyl-9,10-dihydroacridin-10-yl)-2-methylthiopyrimidine (**Comp2**).

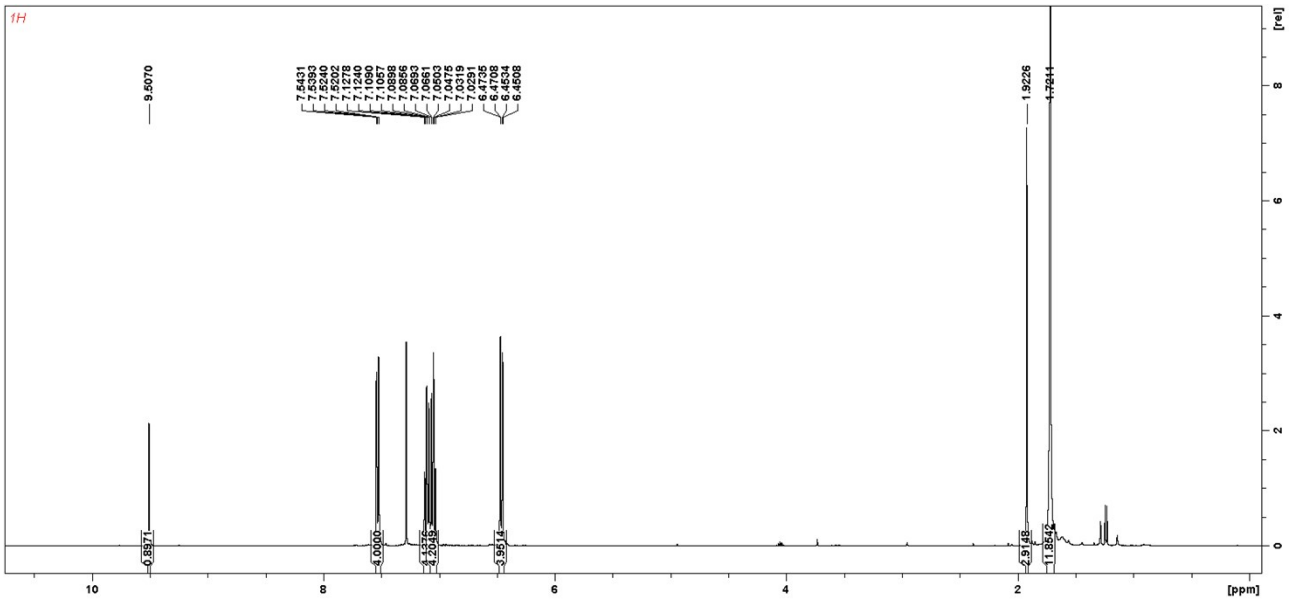

Fig. S10. ^{1}H NMR spectrum of 5-methyl-4,6-bis(9,9-dimethyl-9,10-dihydroacridin-10-yl)pyrimidine (**Comp3**).

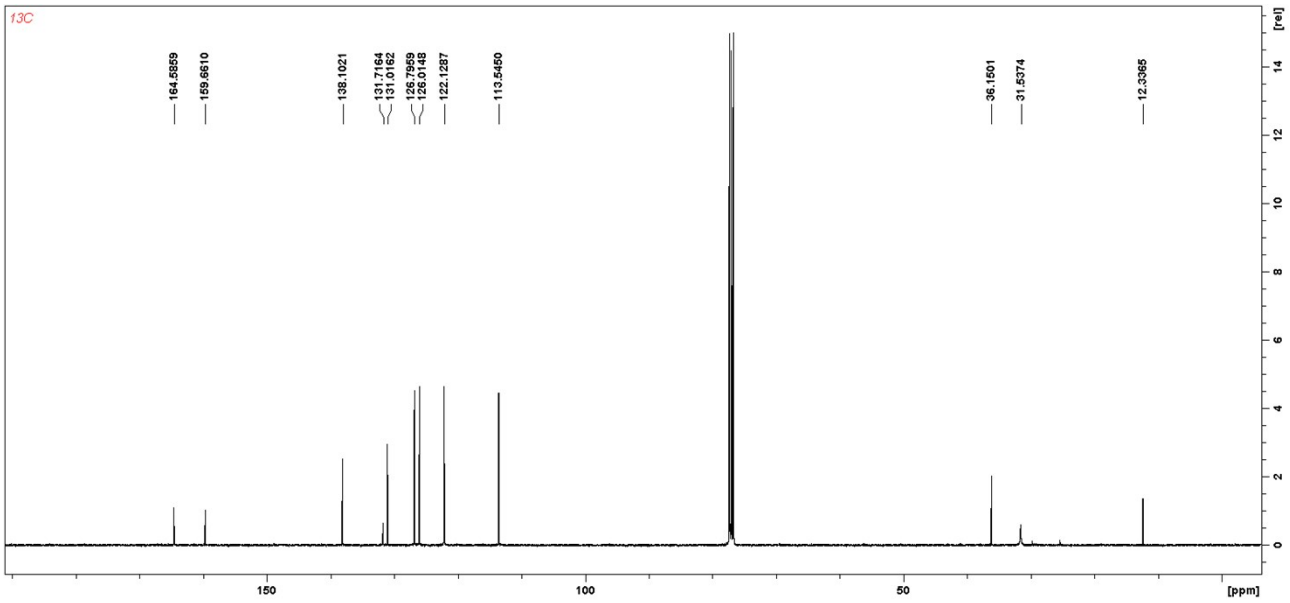

Fig. S11. ^{13}C NMR spectrum of 5-methyl-4,6-bis(9,9-dimethyl-9,10-dihydroacridin-10-yl)pyrimidine (**Comp3**).

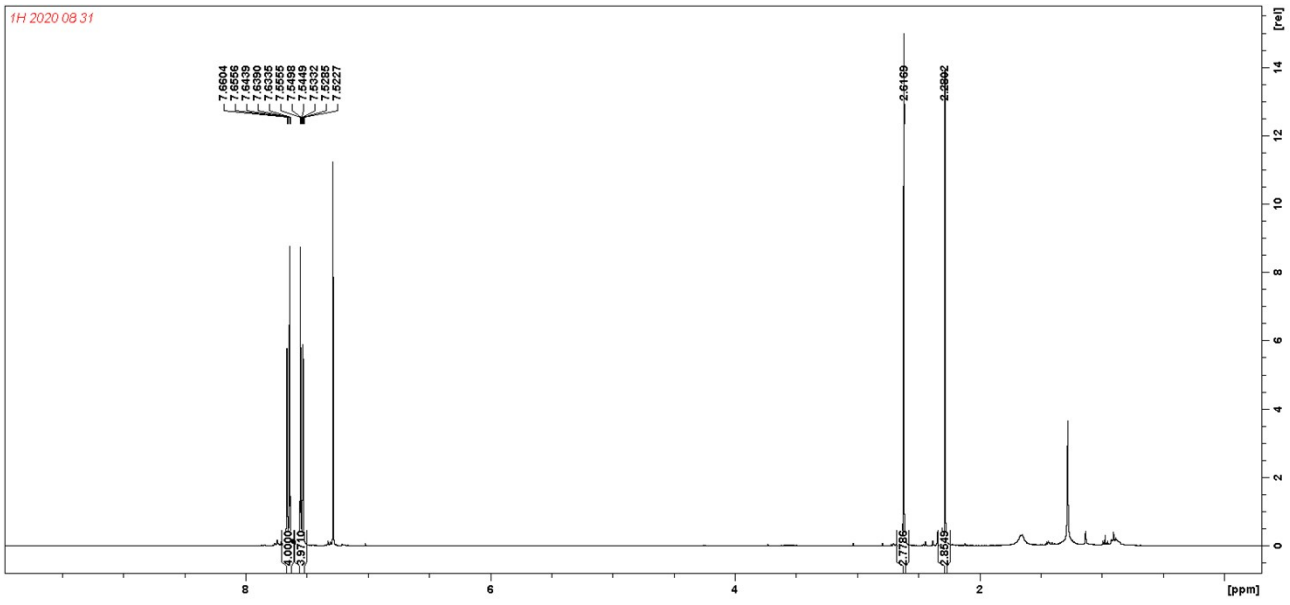

Fig. S12. ^{1}H NMR spectrum of 5-methyl-4,6-bis(4-bromophenyl)-2-methylthiopyrimidine (**5**).

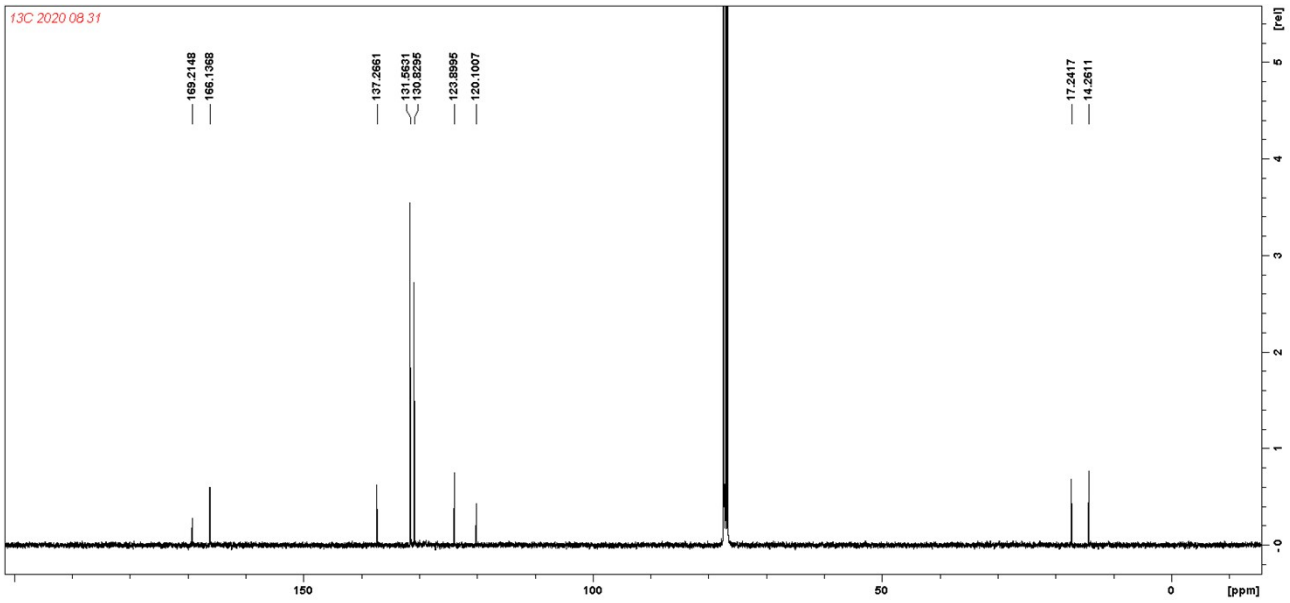

Fig. S13. ^{13}C NMR spectrum of 5-methyl-4,6-bis(4-bromophenyl)-2-methylthiopyrimidine (**5**).

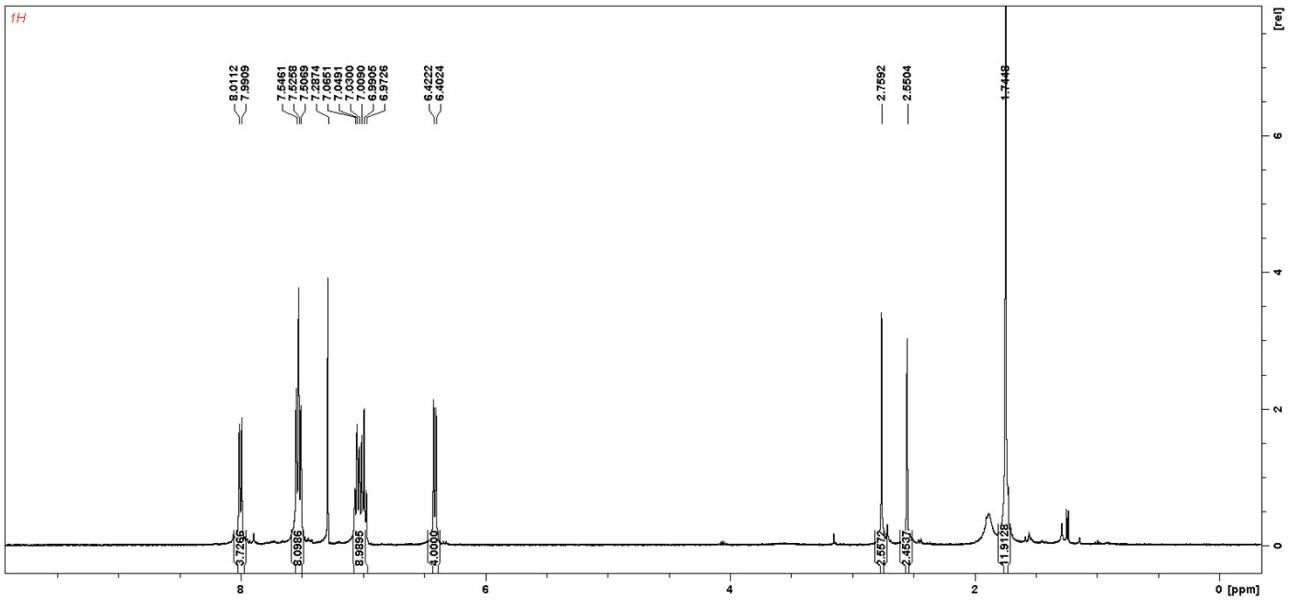

Fig. S14. [1]H NMR spectrum of 5-methyl-4,6-bis[4-(9,9-di-methyl-9,10-dihydroacridin-10-yl)phenyl]-2-methylthiopyrimidine (**ACRphenPyr**).

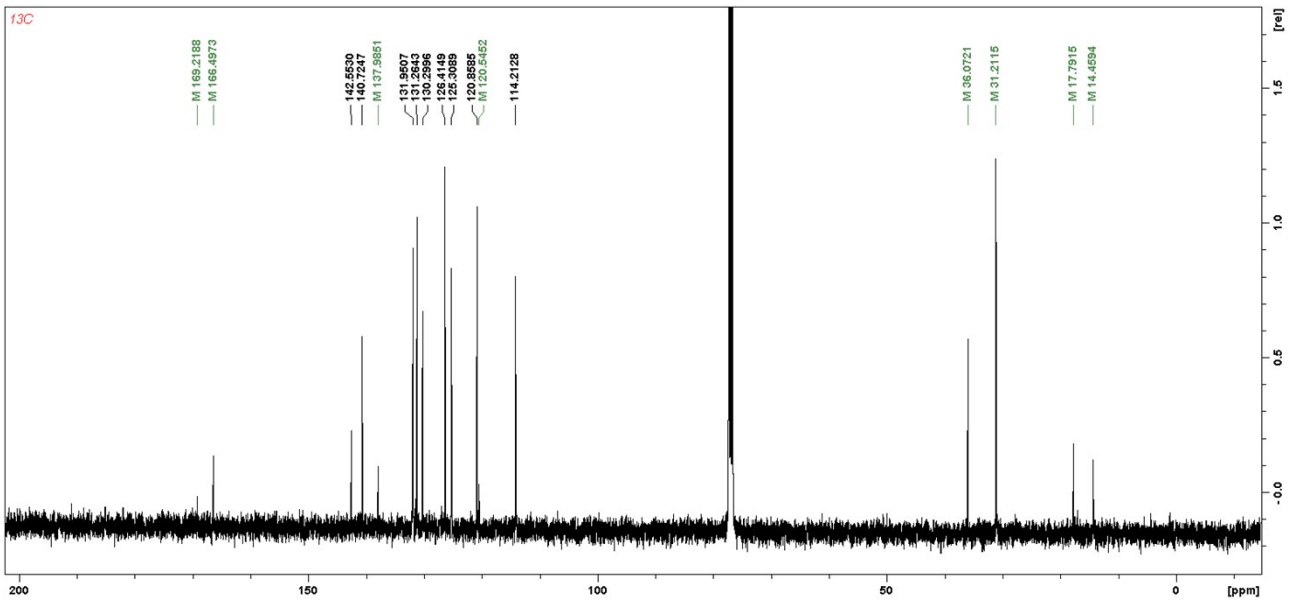

Fig. S15. [13]C NMR spectrum of 5-methyl-4,6-bis[4-(9,9-di-methyl-9,10-dihydroacridin-10-yl)phenyl]-2-methylthiopyrimidine (**ACRphenPyr**).

Structural characterization of intermediate compounds and its emission properties

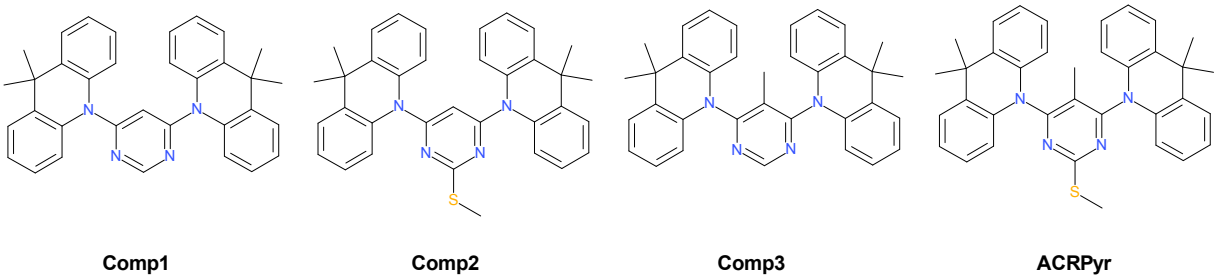

Comp1 Comp2 Comp3 ACRPyr

Comp1

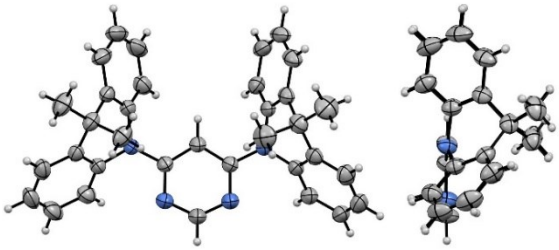

a)

Front view Side view

Comp2

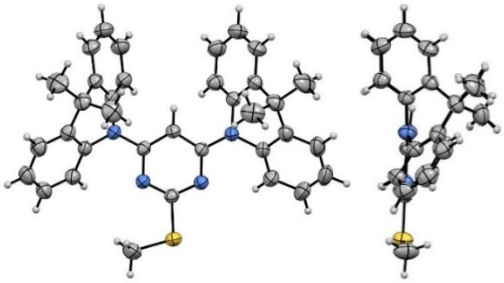

b)

Front view Side view

Comp3

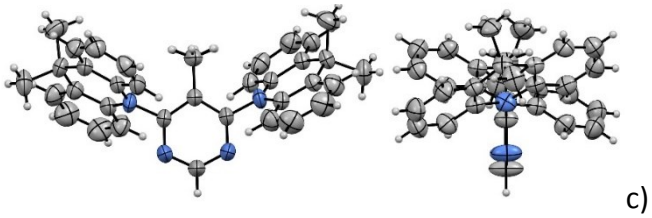

c)

Front view Side view

ACRPyr

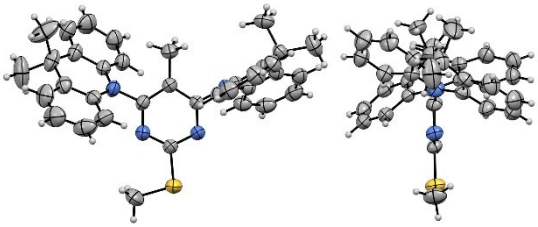

d)

Front view Side view

Fig. S16 X-ray structures of compounds **Comp1**, **Comp2, Comp3** and **ARCPyr** with thermal ellipsoids shown at 50% probability.

Clear domination of TADF-incompatible quasi-axial orientation of ACR unit in acridine-pyrimidine compound **Comp1** was revealed by XRD analysis. The same situation was observed for **Comp2**, having the similar structure as **Comp1** but with sulphur atom at the 2nd position. Quasi-axial orientations of ACR unit were eliminated by introducing 5-methyl unit (**Comp3** and **ACRPyr**).

Table S1. Crystal data and structure refinement details for investigated compounds.

Identification code	Comp1	Comp2	Comp3	ACRPyr
CCDC number	**2016464**	**2014852**	**2016478**	**2010667**
Solvent used	Acetone	Toluene	DMF	Ethanol/H_2O
Empirical formula	$C_{34}H_{30}N_4$	$C_{35}H_{32}N_4S$	$C_{35}H_{32}N_4$	$C_{36}H_{34}N_4S$
Formula weight	494.62	540.7	508.64	554.73
Temperature/K	299.3(6)	299.3(4)	299.5(6)	298.3(3)
Crystal system	monoclinic	monoclinic	monoclinic	monoclinic
Space group	$P2_1/n$	$P2_1/n$	I2/a	$P2_1/c$
a/Å	16.42730(10)	13.04940(10)	16.9071(2)	14.2115(5)
b/Å	9.10160(10)	13.43760(10)	10.62330(10)	7.8920(2)
c/Å	17.97020(10)	16.84160(10)	16.1364(2)	26.2234(8)
α/°	90	90	90	90
β/°	94.4910(10)	96.4340(10)	108.5970(10)	99.051(3)
γ/°	90	90	90	90
Volume/Å^3	2678.56(4)	2934.62(4)	2746.91(6)	2904.52(16)
Z	4	4	4	4
ρ_{calc}g/cm^3	1.226	1.224	1.23	1.269
μ/mm^{-1}	0.563	1.203	0.562	1.229
F(000)	1048	1144	1080	1176
Crystal size/mm^3	0.508 × 0.095 × 0.037	0.347 × 0.194 × 0.041	0.66 × 0.372 × 0.046	0.513 × 0.084 × 0.014
Radiation	Cu Kα (λ = 1.54184)	Cu Kα (λ = 1.54184)	Cu Kα (λ = 1.54184)	Cu Kα (λ = 1.54184)
2Θ range for data collection/°	7.022 to 153.786	8.144 to 153.59	9.99 to 152.6	6.298 to 134.158
Index ranges	$-20 \le h \le 20$, $-11 \le k \le 10$, $-22 \le l \le 21$	$-16 \le h \le 14$, $-16 \le k \le 16$, $-21 \le l \le 21$	$-21 \le h \le 15$, $-12 \le k \le 12$, $-20 \le l \le 20$	$-16 \le h \le 16$, $-9 \le k \le 7$, $-31 \le l \le 31$
Reflections collected	18059	23287	8350	18458
Independent reflections	5457 [R_{int} = 0.0209, R_{sigma} = 0.0219]	6007 [R_{int} = 0.0167, R_{sigma} = 0.0148]	2774 [R_{int} = 0.0145, R_{sigma} = 0.0150]	5200 [R_{int} = 0.0593, R_{sigma} = 0.0560]
Data/restraints/parameters	5457/0/348	6007/0/366	2774/0/182	5200/0/376
Goodness-of-fit on F^2	1.048	1.057	1.106	1.027
Final R indexes [I>=2σ (I)]	R_1 = 0.0384, wR_2 = 0.1082	R_1 = 0.0339, wR_2 = 0.0973	R_1 = 0.0407, wR_2 = 0.1241	R_1 = 0.0508, wR_2 = 0.1264
Final R indexes [all data]	R_1 = 0.0430, wR_2 = 0.1120	R_1 = 0.0366, wR_2 = 0.0995	R_1 = 0.0439, wR_2 = 0.1278	R_1 = 0.0808, wR_2 = 0.1419
Largest diff. peak/hole / e Å^{-3}	0.18/-0.16	0.17/-0.25	0.17/-0.14	0.34/-0.20

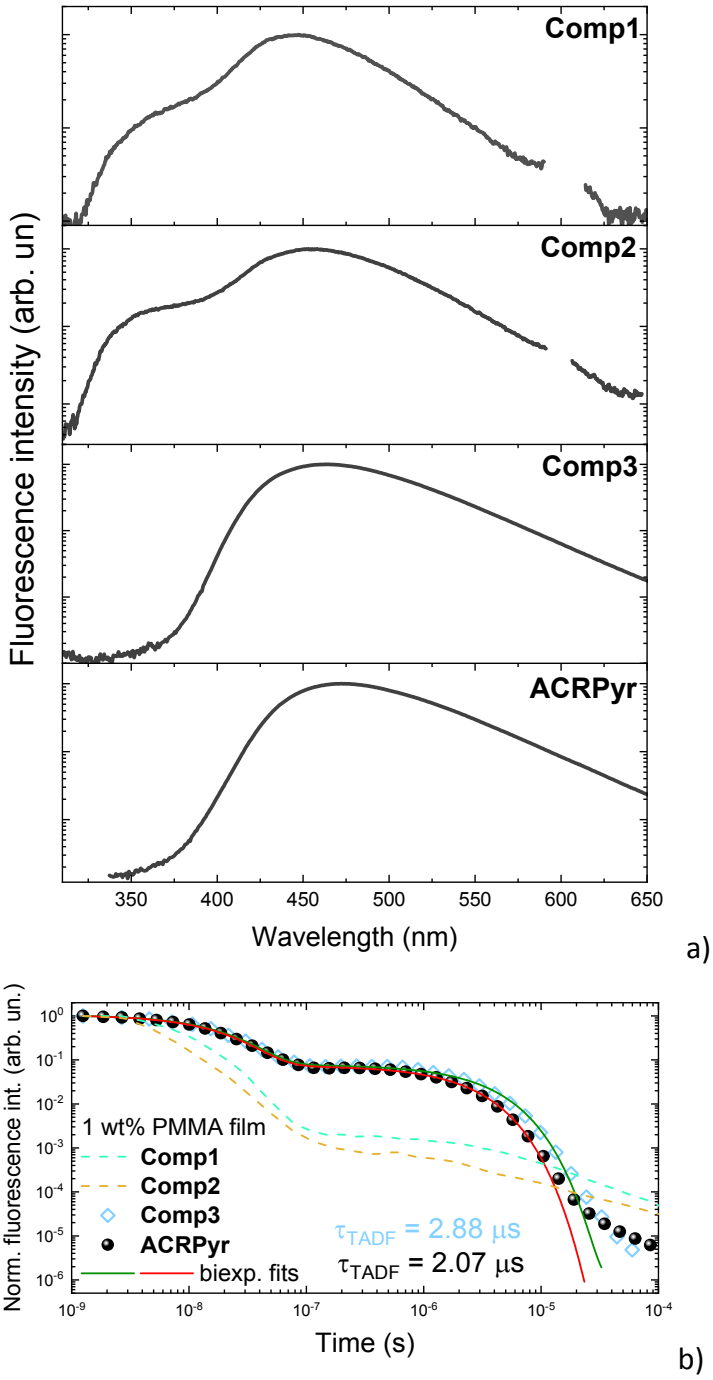

Fig. S17 a) Time-integrated fluorescence spectra of 1 wt% PMMA films of compounds **Comp1**, **Comp2** and **Comp3** in oxygen-free ambient. Emission spectrum of **ACRPyr** was also included for the comparison. We clearly can see that the introduction of 5-methyl unit eliminates the emission of quasi-axial conformers of ACR unit (PL band at about 370 nm). b) Normalized fluorescence decay transients of 1 wt% PMMA films of compounds **Comp1**, **Comp2, Comp3** and **ACRPyr** in oxygen-free ambient. We clearly can see, that the introduction of 5-methyl unit enables the single-exponential DF temporal profile and the further modification of **Comp3** molecular structure with sulphur atom promotes TADF rate, as TADF lifetime decreases from 2.88 μs (**Comp3**) to 2.07 μs (**ARCPyr**)[10]**.**

Thermal properties

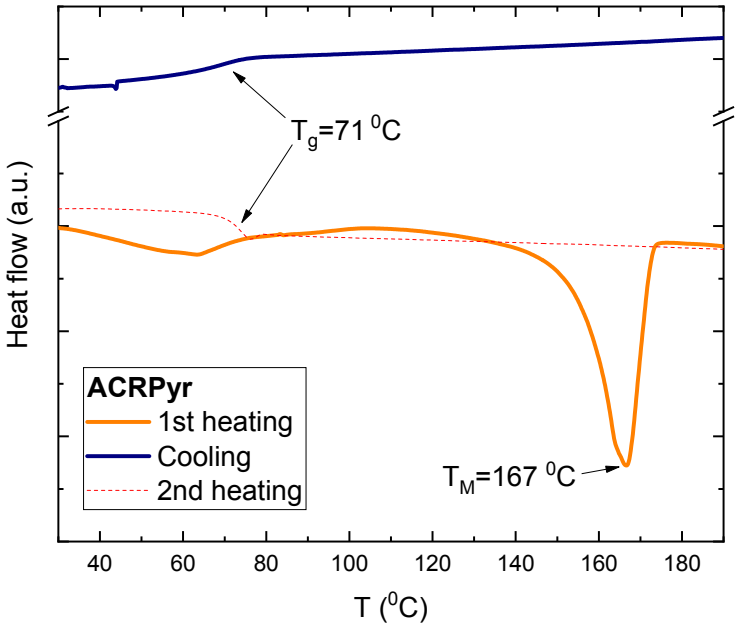

Fig. S18 DSC curves of **ACRPyr**.

Extended photophysical characterization

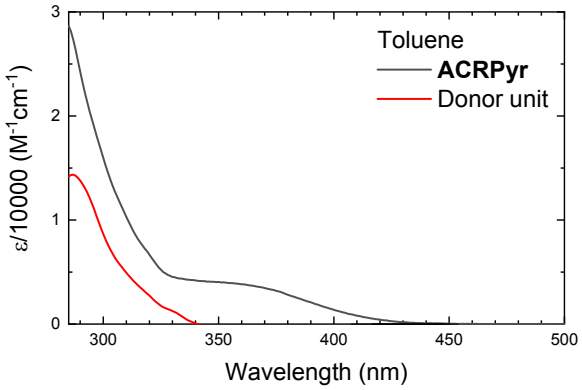

Fig. S19 Absorption spectra of toluene solutions of **ACRPyr** (black line) and donor unit (red line).

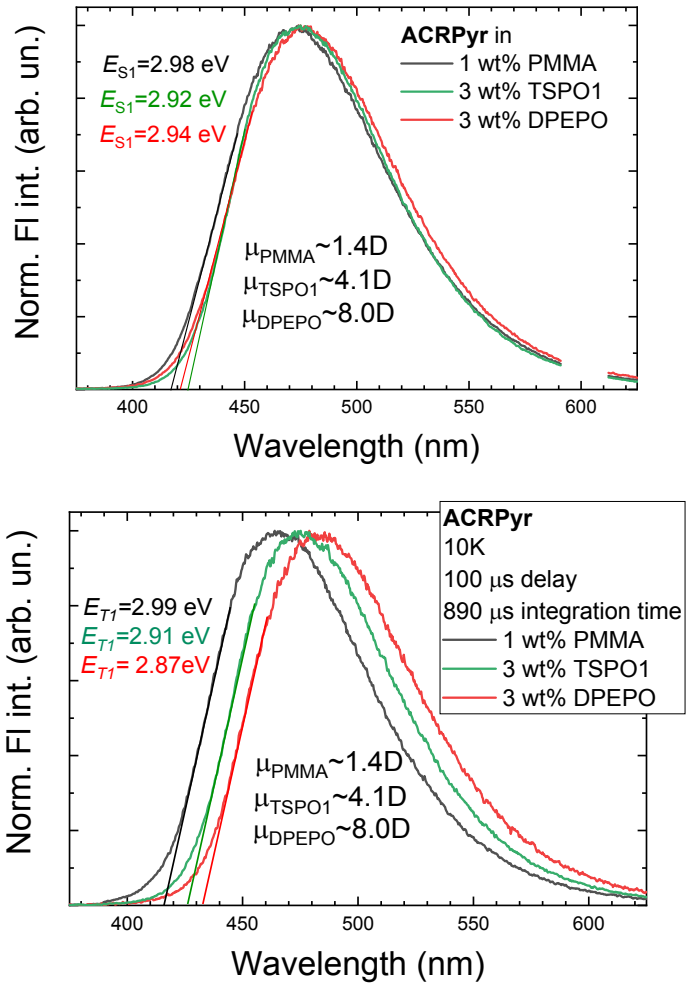

Fig. S20 Normalized fluorescence (upper picture) and 10 K phosphorescence (lower picture) spectra of **ACRPyr** in 1 wt% PMMA (black lines), 3 wt% TSPO1 (green lines) and 3 wt% DPEPO (red lines) films. Dipole moments of PMMA, TSPO1 and DPEPO were of about 1.4[11], 4.1[12] and 8.0 D[13], respectively.

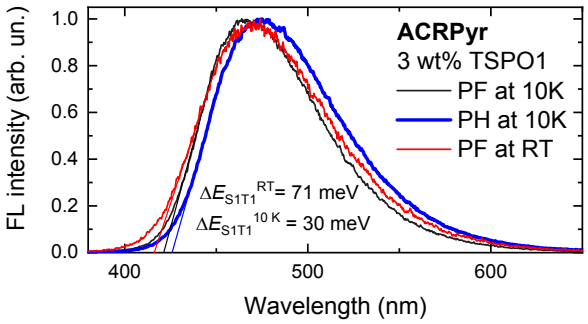

Fig. S21 Normalized time-integrated prompt fluorescence (PF) and phosphorescence (PH) spectra (after 100 µs delay) of 3 wt% TSPO1 films at 10 K temperature. PF spectrum at room temperature is also shown.

a) b)

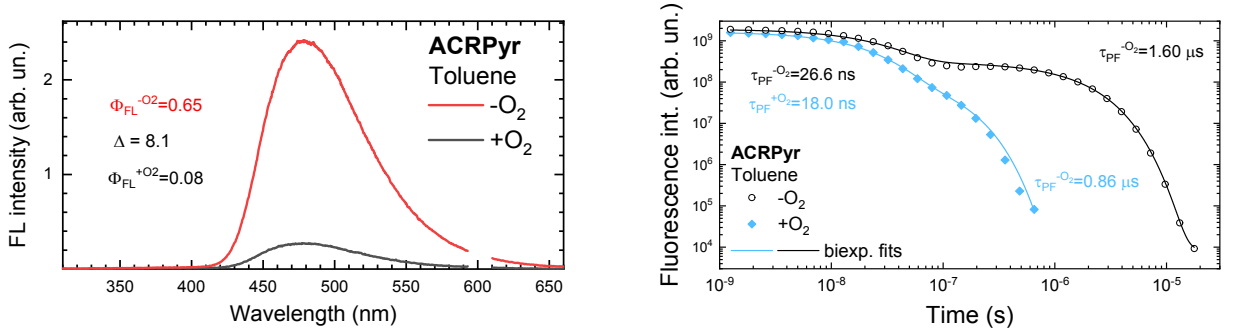

c) d)

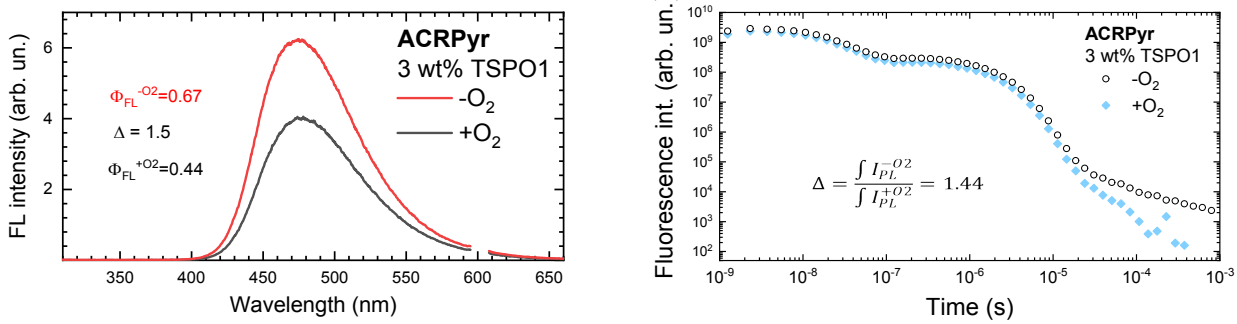

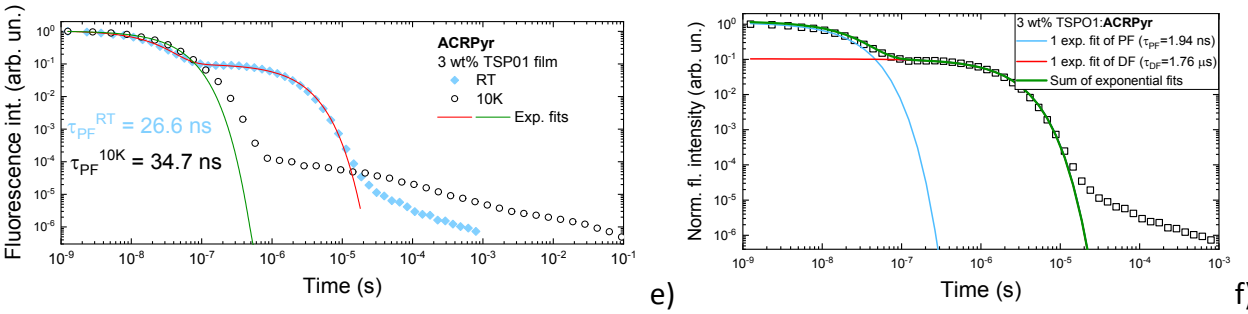

e) f)

Fig. S22 Time-integrated fluorescence spectra of **ACRPyr** in toluene (a) and 3wt% TSPO1 films (c) in oxygen-saturated (black lines) and oxygen-free (red lines) surrounding. Fluorescence decay transients of **ACRPyr** in toluene (b) and 3wt% TSPO1 films (d) in oxygen-saturated (closed figures) and oxygen-free (open figures) surrounding. Figure e shows fluorescence decay transients of 3 wt% TSPO1 film of **ACRPyr** at 10 K (open figures) and room-temperature (closed figures). Solid lines are exponential fits. f) Separate single-exponential fits of prompt and delayed fluorescence of 3 wt% TSPO1:**ACRPyr** film. The corresponding sum of separate fits is also shown (green line).

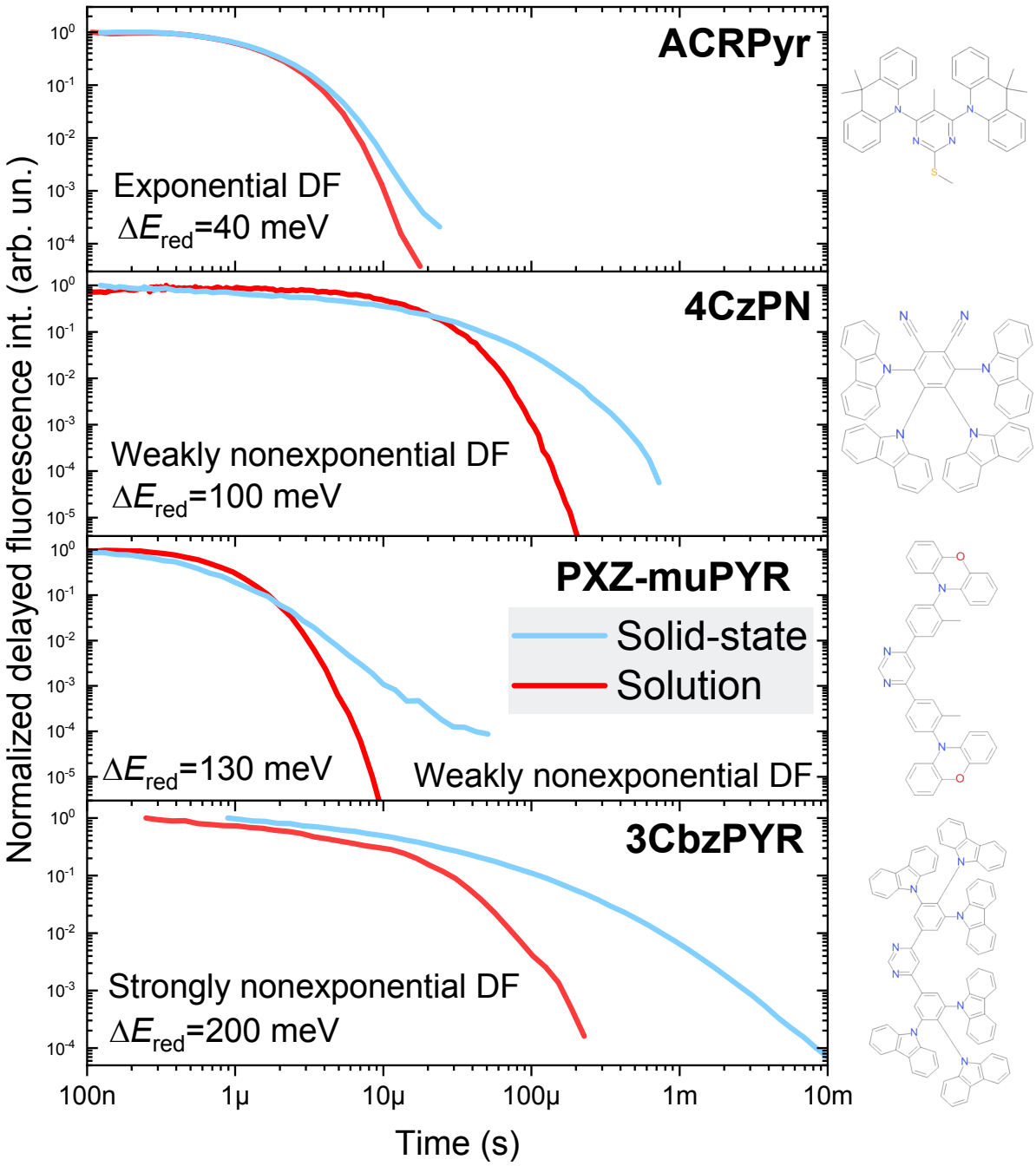

Fig. S23 Normalized delayed fluorescence decay transients of compounds **ACRPyr** (this work), **4CzPN**[7], **PXZ-muPYR**[14] and **3CbzPYR**[15] in oxygen-free solution (red line) and solid-state (light blue line). The size of the initial redshift of PL peak are denoted in the pictures. It is clear, that the larger redshift is in the compounds with the stronger the nonexponential character of temporal profiles of DF transients. On the other hand, larger temporal PL shifts are observed in compounds with more flexible molecular structure[7]. Single-exponential DF decay in solution state is given as guides for eye. Only **ACRPyr** has clear exponential DF profile both in solution and solid-state. Molecular structure of each TADF compound is shown.

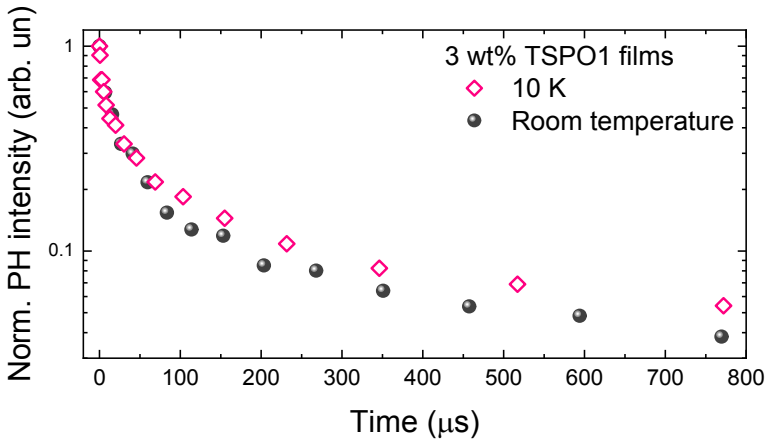

Fig. S24 Phosphorescence decay transients of 3 wt% TSPO1 film of **ACRPyr** at room (closed figures) and 10 K (open figures) temperature. Both transients were taken from Fig. S18 e) and modified accordingly in order to compare their lineshape. The emission intensity was normalized to 1, while the initial decay time was set to 0 μs.

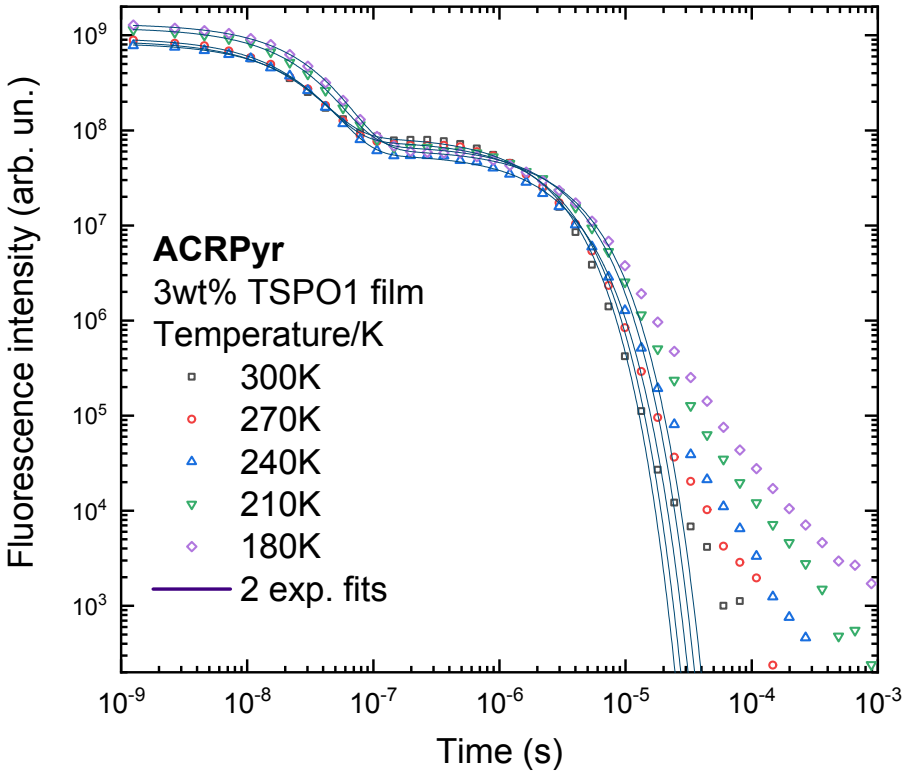

Fig. S25 Fluorescence decay transients of 3 wt% TSPO1 film of **ACRPyr** at different temperature. Solid lines are double-exponential fits.

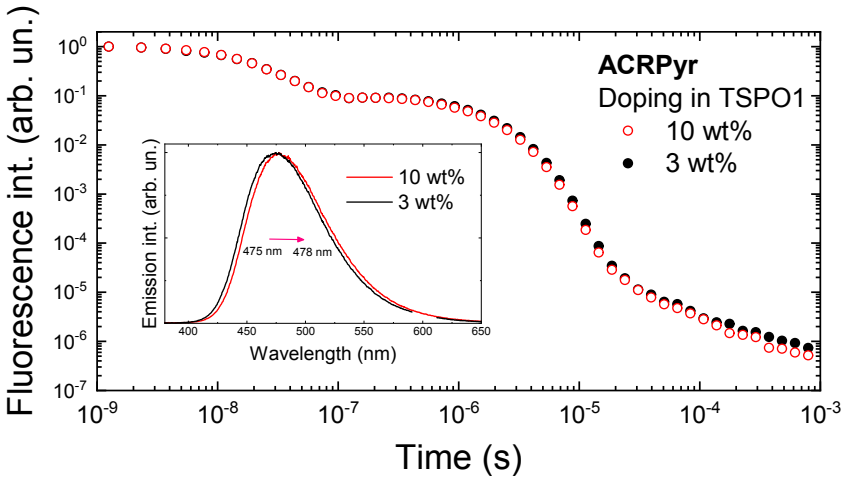

Fig. S26 Normalized fluorescence decay transients of **ACRPyr** in TSPO1 host at 3 wt% (closed figures) and 10wt% (open figures) doping level. The inset shows fluorescence spectra of 3 wt% (black line) and 10 wt% (red line) doped TSPO1 films of **ACRPyr**.

References

1 O. V. Dolomanov, L. J. Bourhis, R. J. Gildea, J. A. K. Howard and H. Puschmann, *J Appl Crystallogr*, 2009, **42**, 339–341.

2 G. M. Sheldrick, *Acta Crystallogr A Found Adv*, 2015, **71**, 3–8.

3 G. M. Sheldrick, *Acta Crystallogr C Struct Chem*, 2015, **71**, 3–8.

4 C. Rothe and A. P. Monkman, *Phys. Rev. B*, 2003, **68**, 1.

5 J. C. de Mello, H. F. Wittmann and R. H. Friend, *Adv. Mater.*, 1997, **9**, 230–232.

6 T. Serevičius, T. Bučiūnas, J. Bucevičius, J. Dodonova, S. Tumkevičius, K. Kazlauskas and S. Juršėnas, *J. Mater. Chem. C*, 2018, **6**, 11128–11136.

7 T. Serevičius, R. Skaisgiris, J. Dodonova, K. Kazlauskas, S. Jursenas and S. Tumkevicius, *Phys. Chem. Chem. Phys.*, 2020, **22**, 265–272.

8 Gaussian 09, Revision D.01, M. J. Frisch, G. W. Trucks, H. B. Schlegel, G. E. Scuseria, M. A. Robb, J. R. Cheeseman, G. Scalmani, V. Barone, B. Mennucci, G. A. Petersson, H. Nakatsuji, M. Caricato, X. Li, H. P. Hratchian, A. F. Izmaylov, J. Bloino, G. Zheng, J. L. Sonnenberg, M. Hada, M. Ehara, K. Toyota, R. Fukuda, J. Hasegawa, M. Ishida, T. Nakajima, Y. Honda, O. Kitao, H. Nakai, T. Vreven, J. A. Montgomery, Jr., J. E. Peralta, F. Ogliaro, M. Bearpark, J. J. Heyd, E. Brothers, K. N. Kudin, V. N. Staroverov, T. Keith, R. Kobayashi, J. Normand, K. Raghavachari, A. Rendell, J. C. Burant, S. S. Iyengar, J. Tomasi, M. Cossi, N. Rega, J. M. Millam, M. Klene, J. E. Knox, J. B. Cross, V. Bakken, C. Adamo, J. Jaramillo, R. Gomperts, R. E. Stratmann, O. Yazyev, A. J. Austin, R. Cammi, C. Pomelli, J. W. Ochterski, R. L. Martin, K. Morokuma, V. G. Zakrzewski, G. A. Voth, P. Salvador, J. J. Dannenberg, S. Dapprich, A. D. Daniels, O. Farkas, J. B. Foresman, J. V. Ortiz, J. Cioslowski, and D. J. Fox, Gaussian, Inc., Wallingford CT, 2013.

9 N. Plé, A. Turck, A. Heynderickx and G. Quéguiner, *Tetrahedron*, 1998, **54**, 9701–9710.

10 Y. Xiang, Y. Zhao, N. Xu, S. Gong, F. Ni, K. Wu, J. Luo, G. Xie, Z.-H. Lu and C. Yang *J. Mater. Chem. C*, 2017, **5**, 12204–12210.

11 M. Shima, M. Sato, M. Atsumi and K. Hatada, *Polym J*, 1994, **26**, 579–585.

12 J. Feng, L. Yang, A. S. Romanov, J. Ratanapreechachai, A. M. Reponen, S. T. E. Jones, M. Linnolahti, T. J. H. Hele, A. Köhler, H. Bässler, M. Bochmann and D. Credgington, *Adv. Funct. Mater.*, 2020, **30**, 1908715.

13 H. Sasabe, Y. Chikayasu, S. Ohisa, H. Arai, T. Ohsawa, R. Komatsu, Y. Watanabe, D. Yokoyama and J. Kido, *Front. Chem.*, 2020, **8**, 427.

14 T. Serevičius, R. Skaisgiris, J. Dodonova, L. Jagintavičius, D. Banevičius, K. Kazlauskas, S. Tumkevičius and S. Juršėnas, *ACS Appl. Mater. Interfaces*, 2020, **12**, 10727–10736.

15 T. Serevičius, J. Dodonova, R. Skaisgiris, D. Banevičius, K. Kazlauskas, S. Jursenas and S. Tumkevicius, *J. Mater. Chem. C*, 2020, **8**, 11192–11200.